

Active vibration control of a smart pultruded fiber-reinforced polymer I-beam

G Song¹, P Qiao², V Sethi¹ and A Prasad³

¹ Department of Mechanical Engineering, University of Houston, TX 77204, USA

² Department of Civil Engineering, University of Akron, OH 44325, USA

³ Department of Mechanical Engineering, University of Akron, OH 44325, USA

Received 12 February 2003, in final form 9 February 2004

Published 1 June 2004

Online at stacks.iop.org/SMS/13/819

doi:10.1088/0964-1726/13/4/020

Abstract

Advanced and innovative materials and structures are increasingly used in civil infrastructure applications. By combining the advantages of composites and smart sensors and actuators, active or smart composite structures can be created and be efficiently adopted in practical structural applications. This paper presents results on active vibration control of pultruded fiber-reinforced polymer (FRP) composite thin-walled I-beams using smart sensors and actuators. The FRP I-beams are made of E-glass fibers and polyester resins. The FRP I-beam is in a cantilevered configuration. The PZT (lead zirconate titanate) type of piezoelectric ceramic patches are used as smart sensors and actuators. These patches are surface bonded near the cantilevered end of the I-beam. Utilizing results from modal analyses and experimental modal testing, several active vibration control methods, such as position feedback control, strain rate feedback control and lead compensation, are investigated. Experimental results demonstrate that the proposed methods achieve effective vibration control of FRP I-beams. For instance, the modal damping ratio of the strong direction first bending mode increases by more than 1000% with positive position feedback control.

(Some figures in this article are in colour only in the electronic version)

1. Introduction

By combining the advantages of composites and smart materials, 'smart composites' or 'intelligent composites' can be created. One reason for this activity is that it may be possible to create certain types of structures and systems capable of adapting to, or correcting for, changing operating conditions. The add-on advantage of incorporating these special types of materials into the structure is that the sensing and actuating mechanism becomes part of the structure by sensing and actuating directly. In recent years, the subject area of 'smart composites' has experienced tremendous growth in terms of research and development.

In the literature, using piezoceramic patch actuators for active vibration control of objects such as small beams has been widely reported; however, vibration control of large objects like in this case of a 3.35 m I-beam is rarely available.

Some reported cases of control of civil structures include that of Makris *et al* (1996) who used an electrorheological (ER) damper for vibration and seismic protection of civil structures. Aizawa *et al* (1998) demonstrated the use of piezoelectric stack actuators for response control of a four-storey structural frame by inserting the actuators into the bottom of a column to produce a bending moment force, and a control algorithm using the model matching method was introduced. They also used electric resistance characteristics of shape memory alloys for sensing damage of a structural member. Krumme *et al* (1995) studied passive control of the dynamic response of civil structures utilizing shape memory alloy (SMA) damping techniques. Kamada *et al* (1997) tested a model of a four-storey building, 3.7 m in height and 2000 kg in total weight, in which 32 stack-type piezoelectric actuators were integrated into the columns for bending moment control. Fujita *et al* (2001) tested a smart structure for active microvibration control

Table 1. Properties of PZT patches used on the beam.

Quantity	Description	Units	QP 40 W	QP 10 W
$L \times w \times t$	Dimensions	cm	$10.16 \times 3.81 \times 0.08$	$5.08 \times 3.81 \times 0.038$
d_{31}	Lateral strain coefficient	$C N^{-1}$	350×10^{-12}	350×10^{-12}
K_3^T	Dielectric constant		3250	1800
ρ_p	PZT density	$kg m^{-3}$	7700	7700
E_p	Young's modulus	$N m^{-2}$	6.9×10^{10}	6.9×10^{10}

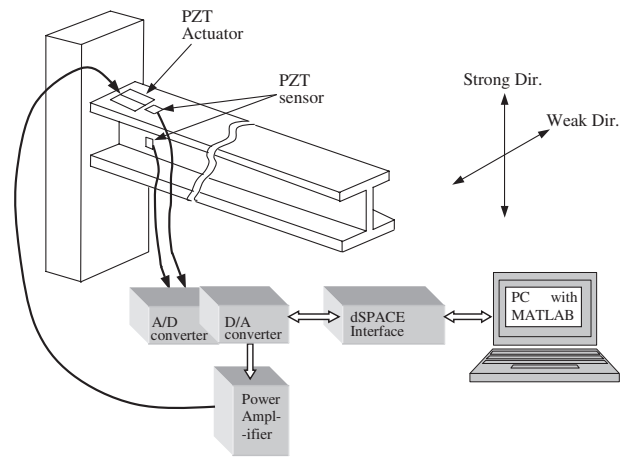
of a two-storey 2500 kg steel frame building model, used in precision manufacturing semiconductor facilities.

The purpose of this experiment is to examine the effectiveness of using smart sensors and actuators for active vibration control of flexible pultruded fiber-reinforced polymer (FRP) composite thin-walled I-beams. Piezoelectric materials will be used as both sensors and actuators in this research since these materials have the advantages of high stiffness, light weight, low power consumption and easy implementation. Piezoelectric materials are primary candidates for dynamic stability applications, such as in resonant vibration, active vibration suppression and dynamic buckling, mainly due to the fact that they tend to have bandwidths beyond the frequency range of structural and acoustic control applications. PZT (lead zirconate titanate) is a commonly used piezoelectric ceramic.

In this research, the object to which we apply active vibration suppression is a pultruded fiber-reinforced polymer (FRP) composite thin-walled I-beam. The FRP I-beam is made of E-glass fibers and polyester resins and is set up in a cantilevered configuration. Three active vibration control methods, positive position feedback (PPF), strain rate feedback (SRF) and lead compensation, are designed and implemented. Positive position feedback (PPF) (Goh and Caughey 1985, Fanson and Caughey 1990, Agrawal and Bang 1993, Baz and Poh 1996, Friswell and Inman 1999, Song *et al* 2000) is applied by feeding the structural position coordinate directly to the compensator, and the product of the compensator and a scalar gain positively back to the structure. PPF offers quick damping for a particular mode provided that the modal characteristics are known. PPF is also easy to implement. Song *et al* (1998) experimentally demonstrated that PPF is robust to a varying modal frequency. Strain rate feedback (SRF) control is used for active damping of a flexible space structure (Newman 1992). Using SRF, the structural velocity coordinate is fed back to the compensator and the compensator position coordinate multiplied by a negative gain is fed back to the structure. SRF has a wider active damping region and can stabilize more than one mode given a sufficient bandwidth. In this research, the SRF is designed to control the vibration of the first mode. A lead compensator if designed properly can increase the damping ratio of a targeted mode by relocating the corresponding dominant pole. Experimental results demonstrate that the PPF, SRF and lead compensation methods are effective in actively increasing damping of the flexible composite I-beam with PZT sensors and actuators.

2. Experimental set-up

The control objective is to show the effectiveness of various vibration suppression strategies for a composite I-beam by using smart sensors and actuators. To achieve this control

**Figure 1.** The experimental set-up (schematic).**Table 2.** Beam properties.

Quantity	Description	Units	Value
L	Beam length	m	3.35
w_b	Beam width	mm	100
h_b	Beam height	mm	102
t_b	Beam thickness	mm	6
ρ_b	Beam density	$kg m^{-3}$	1850

objective an experiment is set up. Its block diagram is shown in figure 1 and the real situation experiment is depicted in figure 2. The 3.35 m long beam is cantilevered at one end and PZT patches are surface bonded to it. Two patches (model No PZT QP-40W) are bonded on each of the top and bottom flange surfaces. These are clearly depicted in figure 1. These PZT patches are used as actuators to excite the beam and to enable active control of the beam vibration. As shown in figure 1, the strong direction refers to the oscillations in the vertical direction whereas the weak direction refers to the oscillations in the horizontal direction. There are also two PZT patches (model No QP-10W) bonded on the beam that act as sensors for the feedback of the signal in the active control algorithms. One sensor is on the top flange for measuring the beam vibration in the strong direction and the other is bonded to the web of the I-beam for measuring its vibration in the weak direction. The properties of the PZT patches are shown in table 1 and the beam properties are shown in table 2.

In this research, we only actively control vibrations along the strong direction of the beam. The vibration suppression algorithm is designed in the MATLAB/Simulink and then downloaded to the dSPACE digital data acquisition and control system for implementation. The dSPACE system is also used



Figure 2. The real situation experimental set-up.

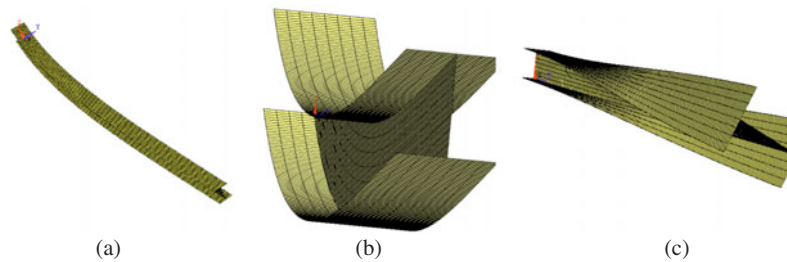


Figure 3. Finite element deformed shapes of: (a) bending along the weak axis; (b) bending along the strong axis; (c) flexural–torsion vibration.

to capture the experimental data. This system comprises a Texas Instruments TMS320C31 floating-point processor. The dSPACE system comes with an analog to digital converter and a digital to analog converter. The dSPACE ControlDesk module is used to develop a graphical user interface (GUI) for online parameter adjustment and real time data acquisition. This module allows one to save the data in the object oriented *.mat format, which is then utilized in Matlab for further processing. Matlab codes were written to analyze the data for modal analysis and energy drops at various modes. The input signals to the PZT actuators in this experiment are amplified using voltage amplifiers, which have an amplification factor of 20. These amplified signals drive the PZT actuators and are used to excite the I-beam. The sensor signals from both the weak and strong directions of the beam are captured and only the strong direction signal is used for feedback control.

3. Finite element modeling and open loop testing

The commercial finite element program ANSYS is used to perform an eigenvalue analysis, and Mindlin eight-node isoparametric layered shell elements (SHELL 99) are employed in the modeling. The finite element deformed shapes for bending along the weak axis and strong axis, and flexural–torsion vibration are given in figures 3(a)–(c), respectively. Analytical frequencies using the exact transcendental and polynomial shape functions along with finite element and experimental results at the length of $L = 3.353$ m are given in table 3. The strong direction refers to the bending along the flanges, the weak direction refers to the bending along the web and the torsional direction refers to the twisting of the beam along the length of the beam. The experimental modal frequency identification is carried out by manually exciting the I-beam in the torsional direction. Vibrational signals measured by the PZT sensors along both weak and strong directions are recorded for power spectral analysis. The power spectral density (PSD) plots of the strong and weak directions of the

manual excitation in the torsional mode are shown below in figures 4 and 5 respectively. The strong direction frequency of 7.62 Hz, the weak direction frequency of 4.49 Hz and the torsional direction frequency of 13.47 are captured and are clearly visible in both the PSD plots of the strong and weak directions. The analytical solution shows a relatively good agreement with FEM and experimental results, especially for the first mode of vibration frequencies. Very close correlations between the analytical and finite element results are achieved.

To experimentally identify the dominant modes of the beam at which the controller should target, more open loop testing was performed. The beam has two main directions of oscillations namely strong and weak directions. The beam was excited by manually tapping at its free end and the data was collected using the GUI based dSPACE ControlDesk. The first test was exciting the beam in its strong direction and the data set was recorded for a period of 25 s. The time response is plotted in figure 6. This data was fast Fourier transformed (FFT) in Matlab so as to generate a power spectral density (PSD) comparison plot (figure 7) for the first 5 s and the last 5 s of the strong direction response during the 25 s data acquisition period. An analysis of the PSD plot for the first and last 5 s revealed that the dominant mode is at 7.62 Hz. The second mode at 45.5 Hz is almost insignificant and dies by itself in 20 s. This leaves us to target control the first mode.

A similar test was performed for the weak direction. The time response and PSD plot are shown in figures 8 and 9 respectively. The analysis of the PSD comparison plot for the first 5 s and the last 5 s of the weak direction response shows that the weak direction dominant mode is at 4.49 Hz. However, the absolute decibel level of the frequency at 4.49 and 28.5 Hz is low and therefore we do not target control of these modes.

Tables 4 and 5 show the comparative decibel levels in the first and last 5 s of the strong and weak direction time responses. Clearly, the high decibel level at 7.62 Hz during

Table 3. Comparison of natural frequencies.

S. No	Mode	Exact transcendental function (Hz)	Polynomial function (Hz)	FEM (Hz)	Experimental (Hz)
1	Weak dir. bending	4.88	4.88	4.81	4.49
2	Strong dir. bending	8.92	8.93	8.83	7.62
3	Torsional dir. bending	13.63	13.55	11.45	13.47

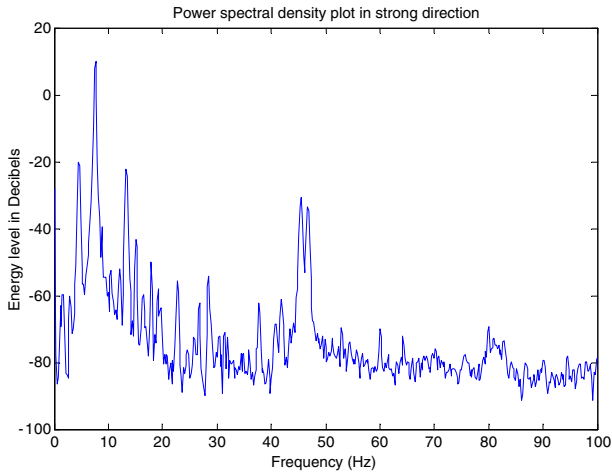


Figure 4. The PSD plot in the strong direction; excitation in the torsional direction.

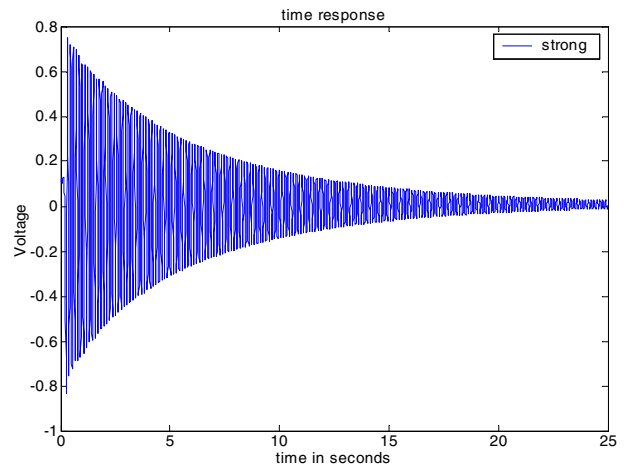


Figure 6. The time response in the strong direction.

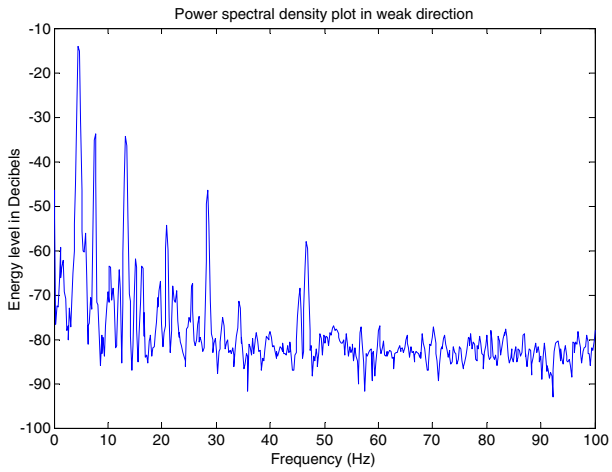


Figure 5. The PSD plot in the weak direction; excitation in the torsional direction.

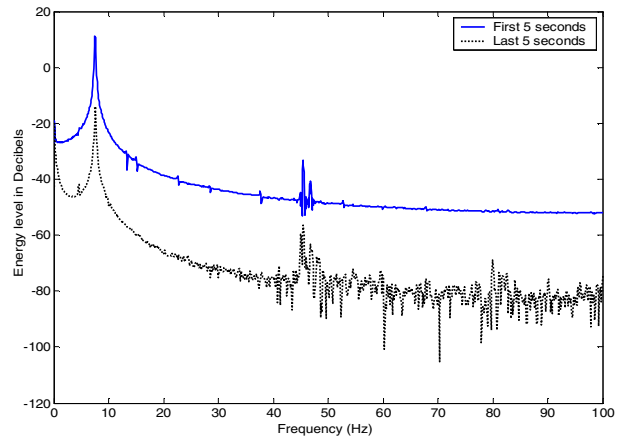


Figure 7. The PSD plot for the first 5 s and last 5 s in the strong direction.

Table 4. The strong direction dB level.

	Frequency	
Decibel level	7.62 Hz	45.5 Hz
First 5 s (dB)	11.1	-33.07
Last 5 s (dB)	-13.95	-56.35

Table 5. The weak direction dB level.

	Frequency	
Decibel level	4.49 Hz	28.5 Hz
First 5 s (dB)	-5.8	-42.2
Last 5 s (dB)	-20.4	-59.8

the last 5 s motivated us to design a controller targeting this strong direction mode.

4. Vibration suppression methods

For this research three vibration suppression methods were used, namely positive position feedback, strain rate feedback and the lead compensation method.

4.1. Positive position feedback control

Positive position feedback (PPF) control was first proposed by Goh and Caughey for the collocated sensors and actuators. Later on Fanson and Caughey demonstrated PPF control in space structures. The PPF control is applied by feeding the structural position coordinate directly to the compensator, and the product of the compensator and a scalar gain positively back to the structure. PPF offers quick damping for a particular

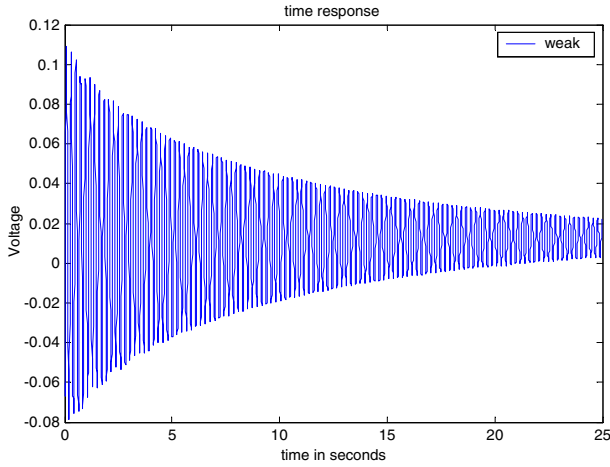


Figure 8. The time response in the weak direction.

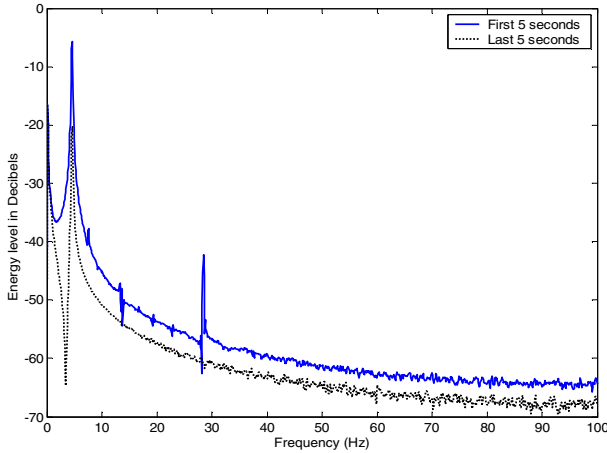


Figure 9. The PSD plot for the first 5 s and last 5 s in the weak direction.

mode provided that the modal characteristics are known. The scalar equations governing the vibration of the structure in a single mode and the PPF controller are given as

$$\ddot{\xi} + 2\zeta\omega\xi + \omega^2\xi = G\omega^2\eta \quad (1)$$

$$\ddot{\eta} + 2\zeta_c\omega_c\dot{\eta} + \omega_c^2\eta = \omega_c^2\dot{\xi} \quad (2)$$

where ξ is a modal coordinate of structure displacement, ζ is the damping ratio of the structure, ω is the natural frequency of the structure, G is the feedback gain, η is the compensator coordinate, ζ_c is the damping ratio of the compensator and ω_c is the natural frequency of the compensator.

The PPF control is illustrated in the block diagram shown in figure 10. In the PPF control, to achieve maximum damping, ω_c should be closely matched to the natural frequency ω of the structure.

4.2. Strain rate feedback control

Strain rate feedback control is implemented by feeding the velocity coordinate to the compensator. The position coordinate of the compensator is then fed back with a negative gain to the structure. When a smart structure is involved using a collocated PZT actuator and sensor, this control is achieved

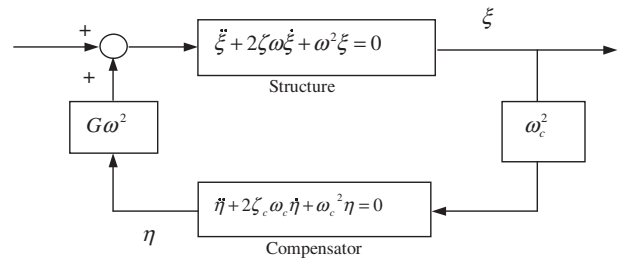


Figure 10. The block diagram of PPF control.

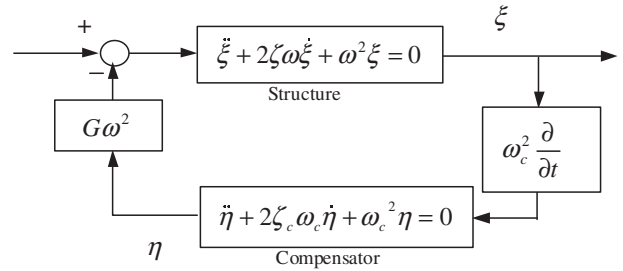


Figure 11. The block diagram of SRF control.

by feeding the derivative of the voltage from the sensor, which is proportional to the strain rate, to the input of the compensator and applying the negative compensator output voltage to the actuator. The scalar equations governing the vibration of the structure in a single mode and the SRF controller are given as

$$\ddot{\xi} + 2\zeta\omega\dot{\xi} + \omega^2\xi = -G\omega^2\eta \quad (3)$$

$$\ddot{\eta} + 2\zeta_c\omega_c\dot{\eta} + \omega_c^2\eta = \omega_c^2\dot{\xi}. \quad (4)$$

The variables above are the same as those defined for PPF control. The block diagram for SRF control is shown in figure 11. In implementing the SRF control the compensator is designed such that the targeted frequencies are below the compensator frequencies. As compared to the PPF, SRF has a much wider active damping frequency region, which gives a designer some flexibility. Selecting a precise compensator frequency for SRF is not as critical as for PPF. As long as the compensator frequency is greater than the structural frequency, a certain amount of damping will be provided.

4.3. Lead compensator

Since the plant (the I-beam) has only one dominant mode the plant can reasonably be assumed to be a second-order underdamped system. The lead compensator is designed for the first dominant mode of the system. The governing equation of the compensator is

$$\text{Lead compensator} = K_c \frac{(s+z)}{(s+p)} \quad |p| > |z| \quad (5)$$

where K_c is the compensator gain, z is the zero and p is the pole of the compensator.

To identify the damping ratio ζ of this mode of the beam the following logarithmic decrement formula is considered:

$$\zeta = \frac{\ln(x_1/x_n)/(n-1)}{\sqrt{4\pi^2 + [\ln(x_1/x_n)/(n-1)]^2}} \quad (6)$$

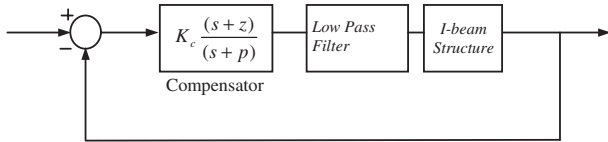


Figure 12. The block diagram of the lead compensator.

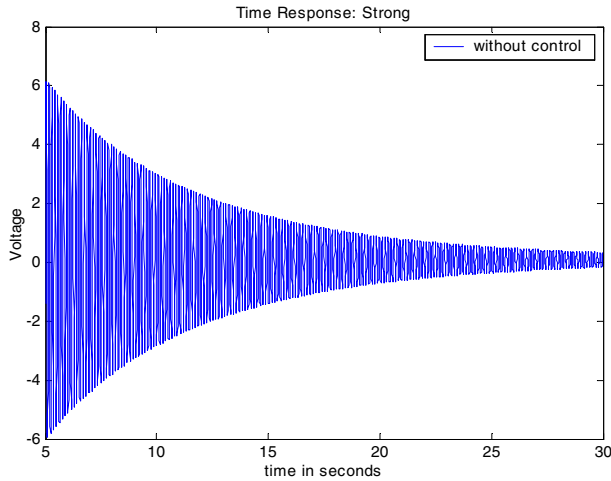


Figure 13. The free response of the beam in the strong direction.

where n is the number of cycles in some time period, x_1 is the amplitude at the beginning of the time period and x_n is the amplitude at the end of the time period. The damping ratio ζ of the dominant mode is found to be 0.0030.

The first natural frequency ω_n of the beam can be calculated using $\omega_n = \frac{\omega_d}{\sqrt{1-\zeta^2}}$ where ω_d is the first damped frequency of the beam as found from the modal testing.

The pole and zero of the compensator can be found by following standard design procedures. The lead compensator can now be represented in a block diagram, as shown in figure 12.

5. Experimental results on active vibration suppression

5.1. PPF experimental results

The positive position feedback control was implemented using the experimental set-up described in section 2. The mode targeted for control was the one at 7.62 Hz. The controller was implemented using the dSPACE real time control system. The sampling frequency for real time control was set to 2 kHz and the sampling frequency for data acquisition was 200 Hz.

Different values of gains were tested. The PPF controller-damping ratio ζ_c was set to 0.5 and the controller frequency ω_c was set at 47.5 rad s⁻¹ (7.62 Hz). The controller-damping ratio ζ_c was chosen as a compromise between damping effectiveness and robustness.

To ensure a fair comparison, the beam was excited by a sinusoidal signal with a combination of white noise for the initial 5 s in both the uncontrolled and controlled cases. Figure 13 shows the free vibrations of the beam after the excitation and figure 14 shows the corresponding PPF controlled vibrations of the beam. The PPF controlled

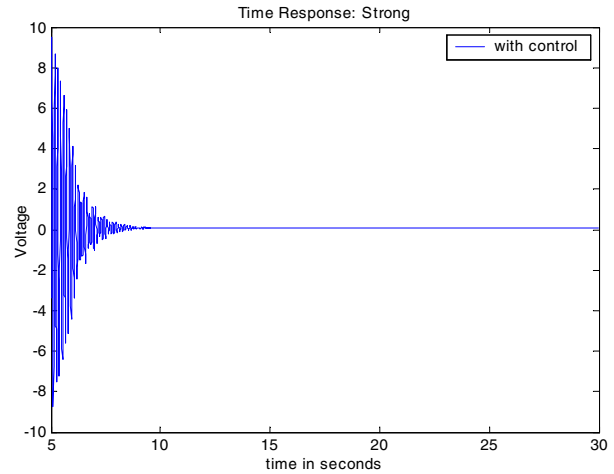


Figure 14. The PPF controlled response of the beam in the strong direction.

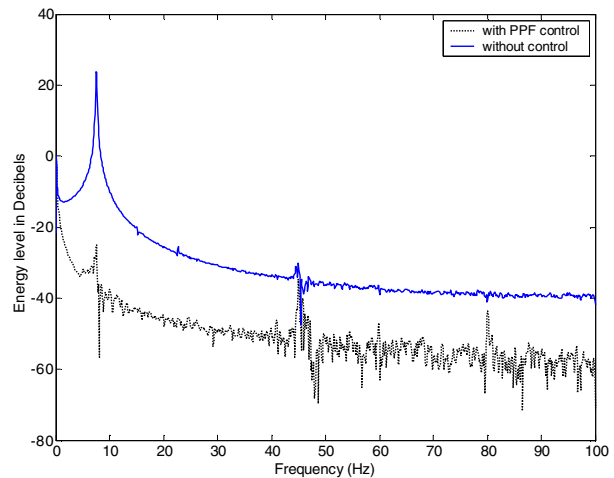


Figure 15. A PSD comparison plot for PPF controlled strong direction vibration of the beam for a 10–15 s period.

Table 6. PPF results.

PPF gain	Modal drop dB 10–15 s	Uncontrolled damping ratio	Controlled damping ratio	Change in damping (%)
0.5	9.85	0.0030	0.0062	106
1.0	24.64	0.0030	0.0112	273
1.5	41.23	0.0030	0.0197	557
2.0	45.22	0.0030	0.0207	590
2.5	51.07	0.0030	0.0383	1177

vibrations of the beam damp out within 5 s after excitation. However, just as the controller kicks in the beam experiences increased amplitude vibrations which soon damp out.

The PSD plot for 10–15 s is shown in figure 15. A drop of 51 dB as compared to the uncontrolled energy level is observed during this period of active control. The corresponding damping ratio as calculated is 0.0383 as against the free vibration damping ratio of 0.0030, which represents an increase of 1176%. A number of tests were conducted with variation in the PPF gain and keeping ζ_c at 0.5 and ω_c at 47.5 rad s⁻¹. The results are shown in table 6, with maximum damping achieved at a gain of 2.5.

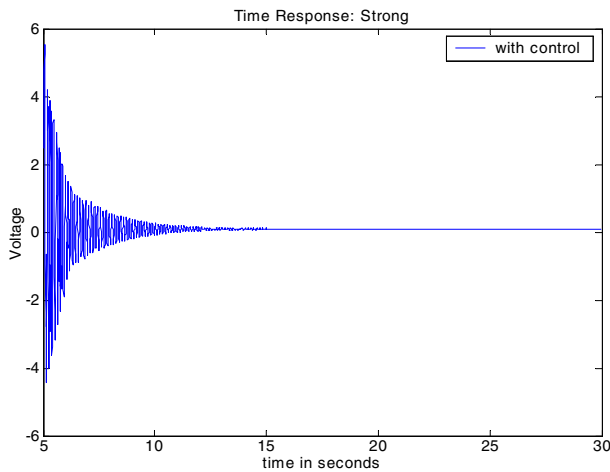


Figure 16. The SRF controlled response of the beam in the strong direction.

Table 7. SRF results.

SRF gain	Modal dB drop 10–15 s	Uncontrolled damping ratio	Controlled damping ratio	Change in damping (%)
-0.01	31.15	0.0030	0.0144	380
-0.02	37.60	0.0030	0.0174	480
-0.03	34.85	0.0030	0.0213	610

5.2. SRF experimental results

The strain rate feedback control was implemented in real time on the beam using the dSPACE system. The mode targeted for control was the dominant frequency of 7.62 Hz. The sampling frequency for real time control was set to 2 kHz and the sampling frequency for data acquisition was 200 Hz.

The SRF controller–damping ratio ζ_c was set at 0.10, controller frequency ω_c was set at 62.83 rad s⁻¹ (10 Hz, which is greater than 7.62 Hz, the targeted mode) and the effectiveness of the SRF controller at various gains was tested.

Similar to in the PPF experiment, the beam was excited by a sinusoidal signal and white noise for 5 s in both the cases of uncontrolled and controlled vibrations. The SRF controlled time response is depicted in figure 16. The beam vibrations die out within 10 s after the excitation signal is stopped. However, the results are not as dramatic as that of PPF, where the vibrations die down within 5 s. In comparison to PPF, in SRF there is no initial overshoot observed. The PSD plot for 10–15 s in shown in figure 17. The SRF control was accompanied with a drop of 34.85 dB in the energy level of the beam in the period of active control. The damping ratio achieved was 0.0213 as against the undamped ratio of 0.0030, which represents an increase of 610%.

Experiments were conducted at different values of the SRF gain with the other parameters as listed above. The results are tabulated in table 7.

5.3. Lead compensator experimental results

The lead compensator was designed using the techniques discussed in section 4.3. The lead compensator designed is

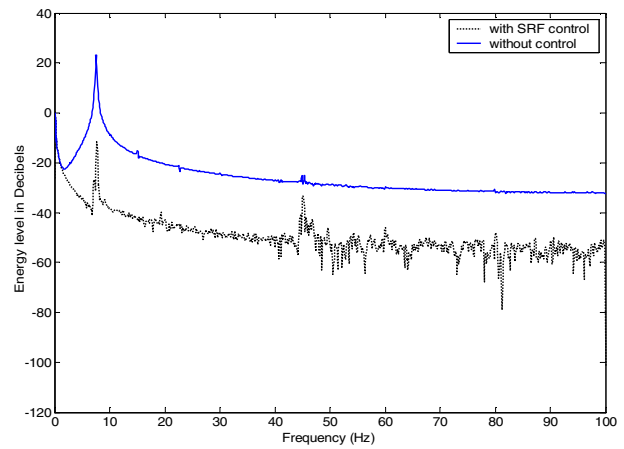


Figure 17. A PSD comparison plot for SRF controlled strong direction vibration of the beam for a 10–15 s period.

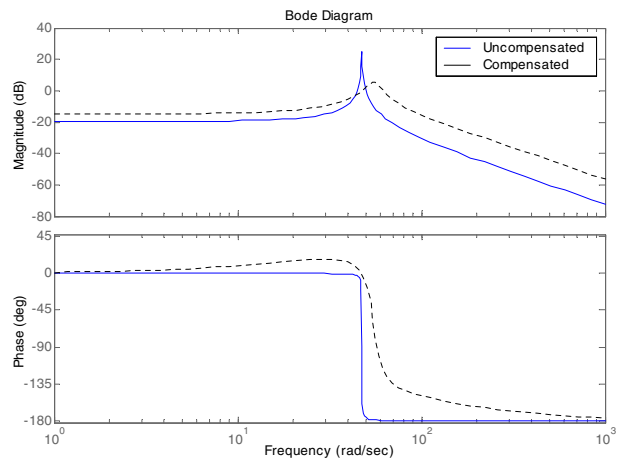


Figure 18. A Bode plot of the lead compensator controlled I-beam and the uncompensated I-beam in the strong direction for gain K_c equal to 6.33.

as follows:

$$\text{Lead compensator} = K_c \frac{(s + 31.69)}{(s + 95.61)}. \quad (7)$$

The designed lead compensator was implemented in real time with a sampling frequency 2 kHz for control and a sampling frequency of 200 Hz for data acquisition. The excitation of the beam was identical to that discussed for PPF and SRF.

At gain K_c equal to 6.33, figure 18 shows the Bode plot and figure 19 shows the pole zero locations of the compensated and uncompensated systems. From the magnitude plot in figure 18 it is clear that the damping of the system is increased, which is indicated by sharp trimming of the peak, and the phase plot shows the increase in the phase margin of the system. Figure 19 shows that the new dominant poles are now located at lines that have the higher damping ratio.

The gain K_c of the beam was varied from 2 to 16 and the results are shown at table 8. The damping increase brought about by the lead compensator is not as dramatic as that in PPF and SRF controls. However, the vibrations damp out after 13 s of excitation. The maximum damping ratio achieved

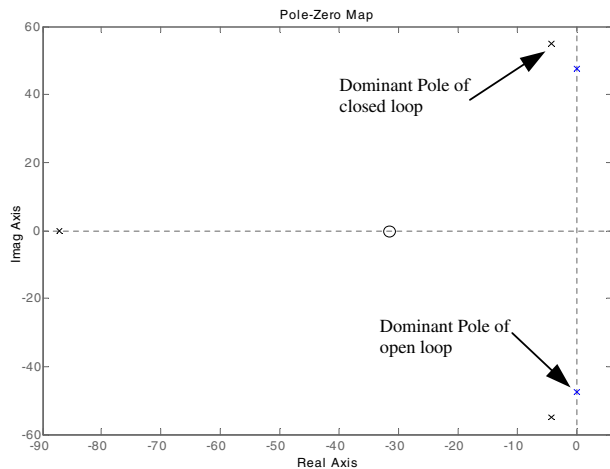


Figure 19. A pole zero map for lead compensator controlled and uncontrolled I-beams in the strong direction. The dominant poles are highlighted clearly for gain K_c equal to 6.33.

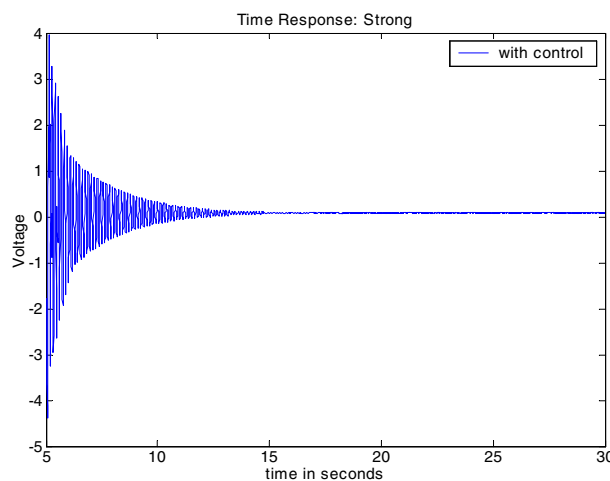


Figure 20. The lead compensator controlled response of the beam in the strong direction.

Table 8. Lead compensator results.

Lead gain	Modal dB drop 10–15 s	Uncontrolled damping ratio	Controlled damping ratio	Change in damping (%)
4	18.95	0.0030	0.0068	127
6	23.45	0.0030	0.0073	143
8	25.55	0.0030	0.0076	153
10	26.70	0.0030	0.0078	160
12	27.80	0.0030	0.0081	170
14	28.21	0.0030	0.0081	170

in this experiment at gain 14 was 0.0081, representing an increase of 170% over the undamped case. There was no initial overshoot observed in this experiment. The time response for the compensated system is shown in figure 20. The PSD plot in figure 21 shows the maximum drop of 28.21 dB in 10 s.

6. Conclusion

The experimental results successfully demonstrated the vibration suppression of a large composite I-beam using PPF,

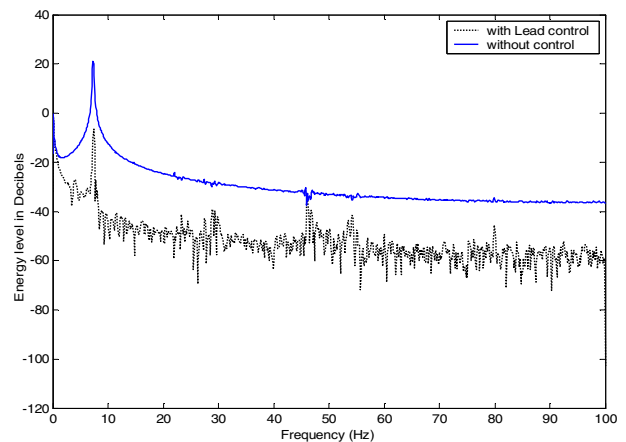


Figure 21. A PSD comparison plot for lead compensator controlled strong direction vibration of the beam for a 10–15 s period.

SRF and lead compensation. Suppression of the single dominant mode vibration was carried out and the best result of an 1176% increase in damping ratio was obtained using PPF control. The PPF was by far the most effective control strategy; however, it is accompanied with initial overshoot. We are now considering designing a fuzzy controller for the initial tuning of the gain, so as to nullify the overshoot observed. SRF results were better than those with the lead compensator but the maximum damping was limited, as the system tends to be unstable at higher gains. The lead compensator was also effective in suppressing the vibrations; however, in this case the modal dB drop was not as significant as compared to the PPF or SRF findings. The damping achieved in this case was limited to 170%, beyond which gain increase caused the system to be unstable. This experiment has the potential to be used in vibration suppression for large composite structural applications in bridges and trusses.

Acknowledgments

The first author would like to express gratitude for the support provided by the NSF via a CAREER grant and NASA via a cooperative grant. The contribution from Dr G P Zou in the modeling of the I-beam is also appreciated.

References

- Agrawal B N and Bang H 1993 Active vibration control of flexible space structures by using piezoelectric sensors and actuators *Vibration and Control of Mechanical Systems* vol 61 (New York: American Society of Mechanical Engineers) pp 169–79
- Aizawa S, Kakizawa T and Higasino M 1998 Case studies of smart materials for civil structures *Smart Mater. Struct.* **7** 617–26
- Baz A and Poh S 1996 Optimal vibration control with modal positive position feedback *Optim. Control Appl. Methods* **17** 141–9
- Fanson J L and Caughey T K 1990 Positive position feedback control for large space structures *Am. Inst. Aeronaut. Astronaut. J.* **28** 717–24
- Friswell M I and Inman D J 1999 The relationship between positive position feedback and output feedback controllers *Smart Mater. Struct.* **8** 285–91
- Fujita T, Enomoto M, Arikabe T, Ogawa T, Murai N, Hashimoto Y, Hamaguchi H and Kitahara T 2001 Active microvibration

- control of precision manufacturing factories with smart structure using piezoelectric actuators *Proc. SPIE-Int. Soc. Opt. Eng.* **4330** 449–59
- Goh C J and Caughey T K 1985 On the stability problem caused by finite actuator dynamics in the collocated control of large space structure *Int. J. Control* **41** 787–802
- Kamada T, Fujita T, Hatayama T, Arikabe T, Murai N, Aizawa S and Tohyama K 1997 Active vibration control of frame structures with smart structures using piezoelectric actuators (vibration control by control of bending moments of columns) *Smart Mater. Struct.* **6** 448–56
- Krumme R, Hayes J and Sweeney S 1995 Structural damping with shape-memory alloys: one class of devices *Proc. SPIE* **2445** 225–40
- Makris N, Burton S and Taylor P D 1996 Electrorheological damper with annular ducts for seismic protection applications *Smart Mater. Struct.* **5** 551–64
- Newman S M 1992 Active damping control of a flexible space structure using piezoelectric sensors and actuators *Master Thesis* US Naval Postgraduate School
- Song G, Schmidt S P and Agrawal B N 1998 Experimental study of vibration suppression of flexible structure using modular control patch *Proc. IEEE Aerospace Conf. (Snowmass, CO, 1998)* (Piscataway, NJ: IEEE)
- Song G, Schmidt S P and Agrawal B N 2000 Active vibration suppression of a flexible structure using smart material and modular control patch *Proc. Inst. Mech. Eng. G* **214** 217–29